# Giant resonances in excited Sn isotopes

D. R. Chakrabarty,* S. Sen, M. Thoennessen, N. Alamanos,† P. Paul, R. Schicker, J. Stachel, and J. J. Gaardhoje‡

*Department of Physics, State University of New York at Stony Brook, Stony Brook, New York 11794*

(Received 22 May 1987)

The giant dipole resonance built on excited states was studied in $^{110,112}$Sn nuclei at excitation energies of 62, 80, 110, and 130 MeV, by measuring $\gamma$ rays following heavy ion fusion reactions $^{16}$O+$^{94}$Mo and $^{19}$F+$^{93}$Nb. The energy of the dipole resonance was found to be 14.8±0.4 MeV independent of excitation energy. This value is approximately 1 MeV below the extrapolated ground state value. The width increases almost quadratically from 6.7 MeV at 62 MeV to 10.8 MeV at 130 MeV. This agrees qualitatively with a theoretical prediction that the increase in width for these nuclei is mainly due to an averaging of strength functions over various oblate shapes induced at high spin and temperature. The sensitivity to the isovector quadrupole vibration was found to be small even at the highest excitation energy. No convincing conclusion could be made for its existence in these Sn nuclei.

## I. INTRODUCTION

The study of the giant dipole resonance (GDR) built on excited states provides the interesting possibility of extracting some fundamental properties of a hot rotating nucleus. This has been made possible[1] by the observation of the GDR strength function in the $\gamma$ decay of highly excited nuclei produced in heavy ion fusion reactions. The energy and width parameters of the GDR depend on nuclear properties such as the symmetry energy, the size and shape of the nucleus, and the degree of coupling of the GDR vibration with the surface vibration modes. For example, a split GDR built on the ground state has been a well established signature for a deformed nuclear shape, and such split GDR has recently been observed[2–4] on excited states as well. A systematic study of these parameters over a wide range in excitation energy and angular momentum makes it possible to follow the evolution of these nuclear properties with spin and temperature. Many theoretical calculations make specific predictions about the change of nuclear shape with spin and temperature, in various nuclei. As different deformed bands become yrast bands (or close to it) with increasing spin, the shape of the excited nucleus can change quite rapidly. At very high spin, near the fission stability limit, superdeformed prolate shapes are predicted in some cases.[5,6] An increase in temperature, in general, produces a reduction of any prolate deformation because of breaking of particle correlations, and leads at sufficiently high $T$ to oblate shapes.[7,8] Various experimental studies of excited state GDR have already addressed and verified some of these predictions.

With a view toward a systematic study over a wide excitation energy range, the present work describes the study of excited state GDR in $^{110,112}$Sn through heavy ion fusion reactions $^{16}$O + $^{94}$Mo and $^{19}$F + $^{93}$Nb. These compound nuclei have spherical ground states. This mass region has previously been studied[9] over an excitation energy of 50–100 MeV where the GDR energy was found to be constant, but the width was observed to increase strongly with excitation energy. The excitation energy range in the present work is 62–130 MeV.

A secondary, but potentially equally important motivation was the search for the isovector giant quadrupole resonance (IVGQR) built on excited states. This mode is expected at 1.6 times the energy of the GDR and its excitation probability is expected to become significant at high excitation energies. A tentative claim has recently been made[9] for the observation of the IVGQR in Sn nuclei at 100 MeV. The present work extends the search for this mode up to 130 MeV excitation energy.

## II. EXPERIMENTAL METHODS AND DATA ANALYSIS

In the present experiment, $\gamma$ rays with energies from 5 to 32 MeV were detected in a large NaI crystal in coincidence with a ten element multiplicity filter. Neutrons were discriminated from $\gamma$ rays by the time of flight technique. The experimental setup is schematically shown in Fig. 1. Self-supporting metallic targets, ~3 mg/cm$^2$ thick, of enriched (94%) $^{94}$Mo and natural $^{93}$Nb were bombarded with $^{16}$O beams of 140 MeV and $^{19}$F beams of 80, 100, and 160 MeV obtained from the Stony Brook LINAC. The beam consisted of bunches $<1$ ns wide with 106 ns bunch separation and was measured in a Faraday cup. Neutron background from the cup was strongly reduced by shielding the beam tube with ~10 cm thick borated polyethylene. The 25.4×38.1 cm NaI(Tl) crystal used for the detection of high energy $\gamma$ rays was placed with its front face at 60 cm from the target, variously at angles of 60, 90, and 120 deg. The crystal was surrounded by a 10 cm thick plastic an-

 

ticoincidence shield. Such shields are routinely used to improve the resolution of a detector for high energy $\gamma$ rays by suppressing the low energy tail of the peak in the spectrum and also to eliminate the cosmic ray background. In the present experiment the latter was the more important function since the intensity of $\gamma$ ray in the spectrum decreases exponentially with energy to a level which, at $\sim 30$ MeV, is less than the cosmic ray background. The detector assembly was surrounded by a 10 cm thick lead shield. A 6 mm thick lead sheet in front strongly reduced low energy $\gamma$ rays and x rays, and attenuated $\sim 15$ MeV $\gamma$ rays to $\sim 70\%$. The $\gamma$ ray multiplicity filter was used to generate a fold condition $N \geq 2$ during data recording in order to emphasize fusion events over inelastic scattering. It consisted of ten $7.6 \times 10.2$ cm NaI detectors mounted at a distance of 15 cm from the target spot. Each front face was covered with 0.2 mm copper, 0.33 mm tin, and 0.25 mm lead. This combination of the absorbers produced a flat (within $\sim 15\%$) relative efficiency of the detectors for $\gamma$-ray energies from $\sim 0.2$ to $\sim 2.5$ MeV. The detectors were wrapped with 3 mm thick lead which reduced Compton cross talk to $< 1\%$. The product of solid angle and efficiency for each element was determined to be $0.011 \pm 0.002$.

In the electronic setup, the summed photomultiplier pulses from the big NaI detector were split into two paths. In the "linear" path, pulses were clipped to $\sim 500$ ns and then fed into two parallel charge sensitive analog-to-digital-converters (ADC's). In the "logic" path, the same pulses were shortened to $\sim 150$ ns and fed into a constant-fraction discriminator (CFD) with adjustable threshold. The output of this discriminator produced (1) the timing pulse for the time of flight measurements, (2) two gating signals of 150 and 600 ns widths, respectively, for the two ADC's, and (3) a logic signal for generating the event trigger. Pulses from the plastic anticoincidence shield were used to veto the event trigger under two conditions. When a high energy $\gamma$ ray is detected in the NaI crystal, a part of the energy may leak out and be absorbed in the plastic. Such events were vetoed in order to improve the resolution of the detector, with an energy threshold of $\sim 1.2$ MeV and a blocking time of $\sim 100$ ns. Cosmic ray $\mu$ mesons passing through the plastic shield deposit at least 5 MeV energy in it. These cosmic ray events were vetoed with a higher energy threshold of $\sim 5$ MeV and a blocking time of 10 $\mu$s in order to eliminate pulses produced by the delayed electron decay of the muons stopped in the crystal. The outputs from the ten multiplicity detectors were fed into a multiplicity logic unit which produced an output signal only when at least two input pulses were present, and simultaneously to a bit register which recorded the firing pattern of the detectors. For the time of flight measurement which discriminates neutrons from $\gamma$ rays, the time-to-digital converter (TDC) was started with the rf pulse from the LINAC and was stopped by the event detected in the crystal. A typical time of flight spectrum is shown in Fig. 2. The event trigger was generated by a coincidence between the logic pulses from the big NaI detector, the rf pulse from the LINAC, and the output of the multiplicity logic unit. For each event, the outputs of the two ADC's, the TDC, and the bit register were sent via a CAMAC crate to a PDP 11/60 computer and recorded on tape.

The energy calibration and the line shape of high energy $\gamma$ rays detected in the large NaI detector were obtained with the reaction $^{11}$B(p,$\gamma$) at $E_p = 7$ MeV. At this proton energy, the reaction produces two $\gamma$ rays of energies 22.37 and 17.94 MeV as shown in Fig. 3. Other energy values used for the calibration were $E_\gamma = 6.83$ MeV from the thermal neutron capture in the NaI detector and $E_\gamma = 4.43$ MeV from $^{12}$C, both seen in the same re-

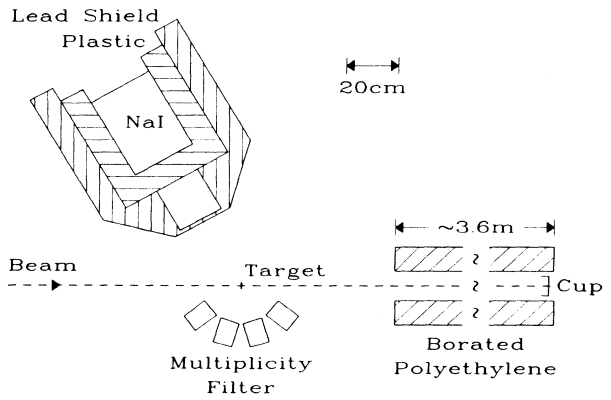


FIG. 1. Schematic diagram of the experimental setup. The multiplicity filter consists of ten $7.6 \times 10.2$ cm NaI detectors.

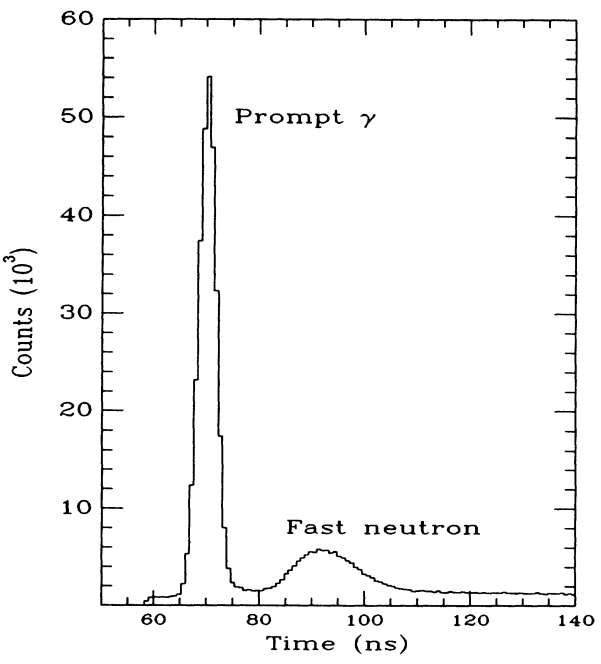


FIG. 2. Time of flight spectrum measured in $^{19}$F + $^{93}$Nb at 100 MeV. Prompt $\gamma$ peak and fast neutron peak are indicated.

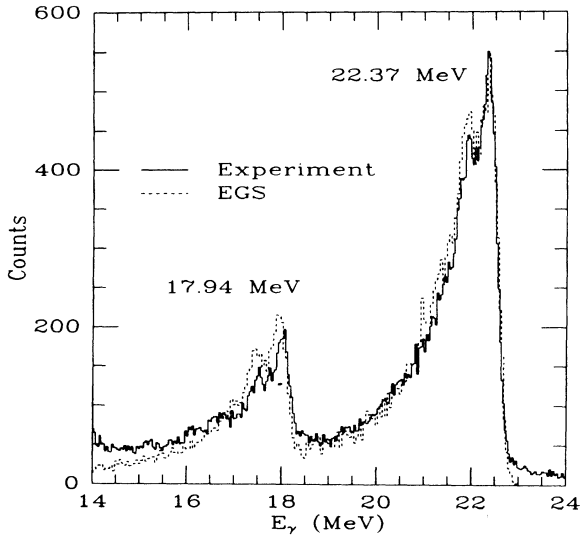


FIG. 3. Gamma spectrum measured in $^{11}$B(p,$\gamma$) at $E_p=7$ MeV. The dashed spectrum is from an EGS calculation for the two peaks at 17.94 and 22.37 MeV.

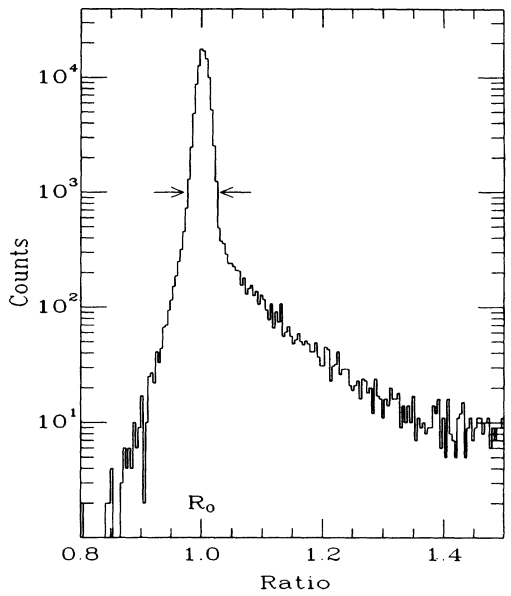


FIG. 4. Ratio spectrum measured in $^{16}O+^{94}Mo$ at 140 MeV. The arrows define the gate around $R_0$ (normalized to 1.0) used in the data analysis for pileup rejection.

action. The resolution apparent in the spectrum of Fig. 3 is worse than can be optimally achieved due to the two deliberately chosen degrading adjustments mentioned above, i.e., firstly, the pulse length was clipped to 500 ns to reduce pileup, and secondly, the energy threshold in the plastic anticoincidence shield was set at relatively high value of $\sim 1.2$ MeV in order to keep the rejection rate at an acceptable level. The line shapes were modeled by the electron gamma shower code (EGS) which produced the fits indicated in Fig. 3. This code was then used to simulate line shapes over the full energy range from 5 to 32 MeV.

The detection and elimination of pileup events in the NaI detector was important for the present experiment. The pulsed time structure of the LINAC beam produces particular pileup problems but also makes it possible to use a simple technique[10] to detect pileup. This consisted of a comparison of the early part of the pulse with the full pulse shape, by using two parallel charge sensitive ADC's. Both ADC's were opened simultaneously but one for only 150 ns, i.e., the rising part of the pulse, the other for 600 ns, i.e., the full pulse length. In the absence of pileup, the ratio of the outputs of the two ADC's had a fixed value independent of the pulse amplitude. A typical ratio spectrum gated with prompt $\gamma$ events is shown in Fig. 4. The sharp peak at $R_0$ contains the events without pileup and the counts in the left and right tail regions are generated by pileup with events from earlier and later beam bursts, respectively. In the data analysis an acceptance window was placed around $R_0$ with a width of $\sim\pm 2\%$. This procedure eliminated pileup from different beam bursts with a sensitivity of 500 keV at 20 MeV and less at lower energies.[10] Pileup with $\gamma$ rays from the same beam burst is not eliminated by this method. This again was important only to a level of $\sim 500$ keV which is the average energy of the yrast transitions dominating the $\gamma$ spectrum. The multiplicity of these $\gamma$ rays in the present reactions was $<15$ and considering the attenuation in the front lead absorber, the pileup probability was estimated to be $<0.04$. The effect of neutron pileup from the same beam burst was negligible because of the small multiplicity ($<5$) and average energy ($\sim 200$ keV) deposited[11] in the crystal. Finally, it was estimated that the maximum systematic error in the extracted giant resonance energy, as introduced by the above pileup effect, is $<50$ keV. This is negligible in comparison with other sources of error discussed later.

The calculation of the absolute cross section for $\gamma$ decay was made from the knowledge of the total efficiency of the NaI detector, beam current, target thickness, acceptance factors of the gates set during the data scan on time of flight (TOF) and ratio spectra, and the efficiency of the multiplicity array. The latter was measured by recording the spectra with and without the multiplicity gate and comparing the yields beyond 12 MeV. Above this energy the spectrum shapes were identical under both conditions.

## III. MULTIPLICITY MEASUREMENTS

The main purpose of the multiplicity filter was the enhancement of fusion events among the event triggers. However, since the firing pattern was included in the event structure, the high energy $\gamma$-ray spectra could be scanned with specific windows on the fold distribution. The measured spectra were found to be independent of the fold number. Conversely, the experimental fold distributions observed in coincidence with high energy $\gamma$

rays were analyzed to extract average multiplicities. These were then compared with the predictions of the statistical model calculations for the decay of the excited compound nuclei, as a check on the consistency of the model.

The spin distribution of the residues following light particle decays, and hence the multiplicity distribution, is decided mainly by the initial spin population in the compound nucleus. In the present procedure for extracting the mean multiplicity, the multiplicity distribution was assumed to be a Gaussian, viz.,

$$F(M)=A\exp\frac{-(M-\overline{M})^2}{2\sigma^2}\ , \tag{1}$$

where $\overline{M}$ is the average multiplicity, $\sigma$ is the width of the distribution and $A$ is a normalization constant. The detailed shape of the distribution was found not to be very important. For example, skewed Gaussian[12] distributions with various amount of skewness resulted in similar fold distributions. This insensitivity was due to the small number of detectors used in the experiment. The mean multiplicity, however, could be extracted with reasonable accuracy by comparing the experimental data with the theoretical fold distribution which can be written as

$$p(n)=\int P_{NM}(n)F(M)dM\ , \tag{2}$$

where[13]

$$P_{NM}(n)=\begin{bmatrix}N\\n\end{bmatrix}\sum_{l=0}^{n}(-1)^{n-l}\begin{bmatrix}n\\l\end{bmatrix}[1-(N-l)\Omega]^M\ . \tag{3}$$

Here $N$ is the number of detectors, $\Omega$ is the efficiency of each and $n$ is the fold. The best values of $\overline{M}$ and $\sigma$ were obtained from the fits by the method of least squares. Figure 5 shows the fold distribution measured at 80, 100, and 160 MeV bombarding energies in the $^{19}F+{}^{93}Nb$ reaction and the best fit to these data. The resultant average multiplicities obtained from these fits are listed in the second column of Table I.

In order to compare the experimental multiplicities with the statistical model calculations, the average residue spin $J_R$ was calculated at different bombarding energies. This was achieved by adding the spin population distributions of all residual nuclei obtained from the fusion evaporation code CASCADE[14] in which the decay step was terminated when the excitation energy was 1 MeV above the yrast band. Assuming that the yrast decay is a mixture of stretched $E2$ and $E1$ (multiplicity $M_1$) and denoting the multiplicity of pre-yrast statistical $\gamma$ rays as $M_S$, the observed multiplicity $M$ can be written as

$$M=M_S+M_1+\frac{J_R-M_1}{2}\ . \tag{4}$$

The values of $M_S$ and $J_R$ obtained from the calculation are shown in the fourth and fifth column of Table I. The third column lists the average values of the spins in the initial compound nucleus. The values of $M_1$ obtained from the Eq. (4) are listed in the last column. It is noted that within the error limits, the values of $(M_s+M_1)$ are consistent with the typical value ($\sim$4) for the total number of $E1$ $\gamma$ rays observed[15] in the deexcitation of deformed compound nuclei. However, the present values have a trend to be larger than four, which again is expected for Sn isotopes which have spherical ground states.

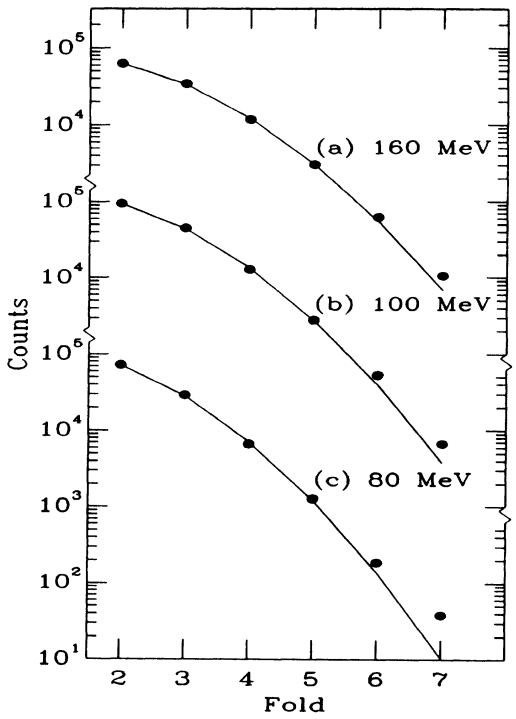


FIG. 5. Fold distribution of $\gamma$ rays measured in the reaction $^{19}F+{}^{93}Nb$ at three energies. Statistical errors are of the size of the data points. The fits shown by the continuous lines are obtained with Gaussian multiplicity distributions with (a) $\overline{M}=16.0$, $\sigma=5.2$ at 160 MeV, (b) $\overline{M}=14.5$, $\sigma=3.9$ at 100 MeV, and (c) $\overline{M}=12.5$, $\sigma=3.3$ at 80 MeV.

## IV. STATISTICAL MODEL CALCULATIONS

The properties of the giant resonances built on excited states were extracted from the comparison of the experimental spectra with the statistical model calculation of the $\gamma$-decay cross sections. To make the numerical aspects of the calculations transparent we list here briefly the salient equations. The decay rate through a particle channel from a particular state $(E_x,J_i)$ of the parent nucleus to a final state $(E_f,J_f)$ in the residual nucleus is given by

$$R_p dE_p=\frac{\rho_2(E_f,J_f)}{h\rho_1(E_x,J_i)}T(E_p)dE_p\ , \tag{5}$$

where $\rho_1$ and $\rho_2$ are level densities in the initial and final nuclei and $T(E_p)$ is the transmission coefficient of the particle of energy $E_p$ carrying the appropriate angular momentum consistent with the conservation of total $J$.

TABLE I. Experimental $\gamma$ multiplicities $M$, computed statistical multiplicities $M_S$ and extracted average $E1$ yrast multiplicities $M_1$ at various bombarding energies in $^{19}F + ^{93}Nb$. $J_{fus}$ and $J_R$ are calculated average angular momenta in compound and residue nuclei, respectively.

| $E_{beam}$ (MeV) | $M$ | $J_{fus}(\hbar)$ | $J_R(\hbar)$ | $M_S$ | $M_1$ |
|---|---|---|---|---|---|
| 80 | 12.5±2.0 | 21.3 | 16.3 | 1.9 | 4.9±4.0 |
| 100 | 14.5±2.5 | 30.2 | 20.2 | 1.9 | 5.0±5.0 |
| 160 | 16.0±2.5 | 43.5 | 21.9 | 1.8 | 6.5±5.0 |

The $\gamma$ decay rate from $(E_x,J_i)$ to a final state $(E_f,J_f)$ can be similarly written as

$$R_\gamma dE_\gamma = \frac{\rho_1(E_f,J_f)}{h\rho_1(E_x,J_i)} F(E_\gamma) dE_\gamma \ . \tag{6}$$

Considering only dipole decay exhausting 100% of the $E1$ classical sum rule strength, the function $F(E_\gamma)$ for the giant dipole resonance (GDR) can be written as

$$F_D(E_\gamma) = 2.09\times 10^{-5} \frac{NZ}{A} \frac{\Gamma_D E_\gamma^4}{(E_\gamma^2 - E_D^2)^2 + \Gamma_D^2 E_\gamma^2} \ . \tag{7}$$

Here $N$, $Z$, and $A$ are the neutron, proton, and mass number, respectively, of the nucleus, and $E_D$ and $\Gamma_D$ are the energy and width of the GDR built on the excited state $(E_f,J_f)$. The function $F_D(E_\gamma)$ is dimensionless and all energies are in MeV.

The hydrodynamical model predicts the isovector giant quadrupole resonance (IVGQR) at an energy $E_{GQ} = 1.6\ E_{GD}$. The strength function for this mode can be included in statistical model calculation in complete analogy to that of the $E1$ mode. The expression for the strength function $F_D$ [Eq. (7)] was derived[16] using a Lorentzian shape for the $E1$ photoabsorption cross section on the excited final state. On the assumption of a Lorentzian photoabsorption cross section also for the IVGQR and using the Gellman-Telegdi sum rule relation for this mode, i.e.,

$$\int \frac{\sigma(E_\gamma)}{E_\gamma^2} dE_\gamma = \frac{\pi^2}{5} \frac{e^2}{\hbar c} \frac{1}{mc^2} \frac{NZ}{A} R^2 \ , \tag{8}$$

one can derive the $E2$ $\gamma$ width as

$$\Gamma_\gamma = \frac{2}{25\pi} \frac{e^2}{\hbar c} \frac{1}{(\hbar c)^2} \frac{1}{mc^2} \frac{NZ}{A} R^2 E_Q^2 \sum_{J_f = J_i - 2}^{J_i + 2} \frac{\rho_1(E_f,J_f)}{\rho_1(E_x,J_i)} \frac{\Gamma_Q E_\gamma^4}{(E_\gamma^2 - E_Q^2)^2 + \Gamma_Q^2 E_\gamma^2} dE_\gamma \ . \tag{9}$$

Here $E_Q$ and $\Gamma_Q$ are the energy and width of the IVGQR and $R$ is nuclear uniform density radius. Expressing energy in MeV and $R$ in fm, the function $F_Q(E_\gamma)$ for the IVGQR becomes

$$F_Q(E_\gamma) = 3.23\times 10^{-11} \frac{NZ}{A} R^2 E_Q^2 \frac{\Gamma_Q E_\gamma^4}{(E_\gamma^2 - E_Q^2)^2 + \Gamma_Q^2 E_\gamma^2} \ . \tag{10}$$

It should be noted that the $E_\gamma$ dependence in both Eqs. (7) and (10) are identical because the photoabsorption cross section for both the modes was assumed to be of Lorentzian shape. In the calculations the total strength function was taken as

$$F(E_\gamma) = F_D(E_\gamma) + F_Q(E_\gamma) \ .$$

For light particle decays only neutron, proton and $\alpha$ decays were considered. However, for high excitation energy and large angular momentum, the fission process becomes important and this was taken into account. The total fission decay probability per unit time is calculated for a liquid drop model of the nucleus as[17]

$$R_{fiss} = \frac{1}{h\rho(E_x,J_i)} \int_0^{E_x - E_B(J_i)} \rho[E_x - E_B(J_i) - E_s, J_i] dE_s \tag{11}$$

and $E_B(J_i)$ is defined by

$$E_B(J_i) = E_{FB}(J_i) + \frac{\hbar^2}{2\mathcal{J}} J_i(J_i+1) \ . \tag{12}$$

Here $E_{FB}$ is the fission barrier in the angular momentum state $J_i$ calculated for a rotating liquid drop, $\mathcal{J}$ is the moment of inertia and $E_s$ is the kinetic energy at the saddle point.

Finally, the level density at the excitation energy $E_x$ and spin $J$ was calculated from the expression

$$\rho(E_x,J) = \frac{\sqrt{a}}{12} \left[\frac{\hbar^2}{2\mathcal{J}}\right]^{3/2} \frac{2J+1}{(U_J+T)^2} \exp(2\sqrt{aU_J}) \ , \tag{13}$$

where

$$U_J = E_x - \Delta - \frac{\hbar^2}{2\mathcal{J}} J(J+1) \ , \tag{14}$$

and the temperature $T$ is defined by $U_J = aT^2 - T$.

## V. RESULTS AND DISCUSSIONS

It is known from earlier measurements[1] that the high energy $\gamma$ rays from fusion evaporation reactions are essentially emitted isotropically. In the present work, this was checked in the reaction $^{16}O + ^{94}Mo$ at 140 MeV by measuring the $\gamma$ ray yield and spectra at 60°, 90°, and

120° with respect to the beam axis. No change was observed in the shape of the spectra at different angles and within statistical errors the yield of $\gamma$ rays was isotropic ($a_2 = -0.02 \pm 0.1$) over the range $E_\gamma = 8-22$ MeV. This can be explained under the assumption of a spherical shape of the excited compound nucleus and a high spin for the initial state. The compound nucleus is, of course, produced in an aligned state in the heavy ion reaction and retains most of the alignment over the different decays steps. In such a condition the $a_2$ coefficient for the dipole angular distribution becomes $-0.25$ for the stretched ($\Delta J = \pm 1$) transition and $+0.5$ for the nonstretched ($\Delta J = 0$) one, in the limit of high spin. For a spherical nucleus the relative probabilities of stretched and nonstretched transitions depend only on the final state level densities. It so happens that the level densities of the states with spin $J-1$ and $J+1$ almost add up to twice that of the states with spin $J$, thus producing isotropy. In view of the observed isotropy most of the data were taken at 120° because of the relatively lower yield of neutrons at backward angles.

In the analysis, the energies and widths of $E1$ and $E2$ giant resonances were extracted from the best fits to the experimental data. These were treated as input parameters in the CASCADE calculations. Other important parameters in the calculations were the fusion cross sections and level density parameters. In the absence of experimental measurements calculated fusion cross sections had to be used and two quite successful models were considered. These are the extra push model[18] and the surface friction model[19] which, however, for the present systems make divergent predictions at the higher bombarding energies. The CASCADE calculations were done with the mean values from two predictions (see Table II), since the shape of the calculated $\gamma$ spectrum was found not very sensitive to the input fusion cross section over a reasonable range.

The choice of the parameters $a$ and $\Delta$ [Eqs. (13) and (14)] in the calculation of the level densities followed the prescriptions given in the code CASCADE. The value $a = A/8$ MeV$^{-1}$ for high excitation energies has been widely used[1] in the literature. Recent experiments[20] on $n$ and $\alpha$ evaporations demonstrate that $A/8$ should be valid up to an excitation energy of $\sim 140$ MeV in the reactions studied in this work. However, in fitting the present $\gamma$ spectra we found that the choice $a = A/9$ gave better results although the fits obtained with a range of $A/8$ to $A/10$ could not be discarded when all four excitation energies were considered. The fitting procedure consisted of stepping energies and widths in steps of 0.1 MeV and comparing the computed spectrum (folded with the $\gamma$ line shape) to the experimental one. The best fit was chosen by visual inspection. A procedure described below allowed this to be done in a sensitive way.

The best fits to the experimental spectra at different bombarding energies are shown in Fig. 6. The solid lines show the fits from the calculations containing only the GDR, but no GQR, strength function. The excess yield below $\sim 7$ MeV region in the data is an artifact from incomplete subtraction of the slow neutron capture events. The calculations were done at an excitation energy corresponding to the beam energy at the middle of the target. Above 8 MeV the calculated spectra were compared to the experimental ones on an absolute scale. The error in the experimental cross sections was estimated to be $\pm 20\%$. The absolute scale in the calculated spectra are determined by the fusion cross sections and the sumrule strength of the GDR. The present fits, using the fusion cross sections listed in Table II and 100% sum rule strength for GDR [Eq. (7)], required an overall normalization factor varying between 0.9 and 1.3, at various excitation energies.

The quality of the various fits can be judged more sensitively from a representation which allows to show the data and the fit on a linear scale. This is achieved by dividing both the experimental and the fit cross sections by a spectrum which is calculated using the same parameters but a constant $E1$ strength function of arbitrarily 0.2 W.u. These "divided" plots are shown in Fig. 7. They demonstrate the generally good quality of fits up to $E_\gamma \sim 25$ MeV. However, structure is clearly present in the data which cannot be reproduced by a single Lorentzian. The deviations from a single Lorentzian shape is particularly apparent at the highest energy. The energy and width parameters of the GDR obtained from the fits using $a = A/9$ are listed in Table II. The errors were estimated from the visual inspection of the sensitivity of the fits to the change of these parameters, keeping the level density parameter unchanged at $A/9$. The width listed for the highest excitation energy is larger by 0.3 MeV than that of the single Lorentzian and was calculated as the half-maximum width of the $E1$ strength function used in the fit shown by the dashed curve in Fig. 7. This dashed curve contains a $E1$ component at $E = 8.8$ MeV with $\Gamma = 3$ MeV and a relative strength of only 5%. It should be mentioned that this structure at $\sim 9$ MeV is present also in the spectra generated with higher fold conditions.

One of the motivations of the present work was to

TABLE II. Energy ($E_D$) and width ($\Gamma_D$) of GDR extracted at different excitation energies in $^{110,112}$Sn. All energies are in MeV.

| Reaction | $E_{beam}$ | $E_{ex}$ | $\sigma_{Fus}$ (mb) | $E_D$ | $\Gamma_D$ |
|---|---|---|---|---|---|
| $^{19}$F + $^{93}$Nb | 80 | 62.2 | 700 | 14.9±0.3 | 6.7±0.4 |
| $^{19}$F + $^{93}$Nb | 100 | 79.3 | 1100 | 14.7±0.3 | 7.9±0.4 |
| $^{16}$O + $^{94}$Mo | 140 | 110.2 | 1335 | 14.9±0.3 | 9.8±0.5 |
| $^{19}$F + $^{93}$Nb | 160 | 130.0 | 1380 | 14.6±0.4 | 10.8±0.6 |

search for the IVGQR. The possibility that IVGQR strength may be present in the spectra at high excitation energy has recently been considered by Gaardhoje *et al.*[9] Based on the scarce ground state systematics,[21] the predicted energy of this mode is $E_Q = 130/A^{1/3} = 27.3$ MeV for $A = 110$. Using a GQR strength function with $E_Q = 27$ MeV, $\Gamma_Q = 8$ MeV, and $S = 100\%$ classical sumrule produces the dotted curves shown in Fig. 6 for the 110 and 130 MeV excitation energy data. Thus the evidence for the IVGQR cannot be ruled out in the present data. However, as can be seen from the fits, even 100% IVGQR does not make a pronounced change in the spectrum shape due to the increase in the GDR width at higher energy. This makes a definite conclusion difficult. The strength which appears only as some excess over the Lorentzian tail of the GDR, could also be due to the redistribution of the GDR strength toward the high tail region at high temperature.[22] Moreover, the cross section above $E_\gamma = 22$ MeV can also be raised by using a level density parameter $a = A/10$.

We now discuss the results on the energies and widths of the GDR. The values obtained in the present work, and the widths reported recently by Gaardhoje *et al.*[9] for the same mass region are plotted in Fig. 8 as a function of excitation energy in the compound nucleus. Within experimental errors, the energy of the excited state GDR is independent of excitation energy. For comparison, Fig. 9 gives the experimental systematics of the energy of the ground state GDR in this mass region[23,24] together with the average energy of the excited state GDR obtained in the present work. The error (±0.4 MeV) shown on the latter includes also the effect of the variation of level density parameter in the range of $a = A/8$ to $a = A/10$. It is noteworthy that the excited state value lies about 1 MeV below the value extrapolated from the ground state systematics. This lowering in the GDR energy could be due to a reduction of symmetry energy with increasing spin or temperature (although in the excitation energy range of this work no such reduction is apparent), or due to a lowering of the ground state symmetry energy for the very neutron deficient isotopes.

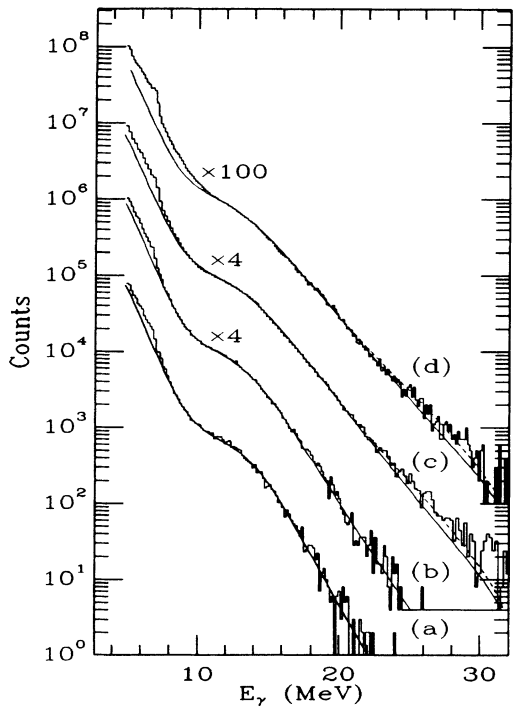


FIG. 6. Experimental data and CASCADE fits in (a) $^{19}F + ^{93}Nb$ at $E_{beam} = 80$ MeV, (b) $^{19}F + ^{93}Nb$ at $E_{beam} = 100$ MeV, (c) $^{16}O + ^{94}Mo$ at $E_{beam} = 140$ MeV, and (d) $^{19}F + ^{93}Nb$ at $E_{beam} = 160$ MeV. The solid curves are obtained with only the GDR strength function using the level density parameter $a = A/9$. The dashed curves at higher energies include also the IVGQR strength function. The fit parameters are listed in Table II (see text).

It can be seen from Fig. 8 that the width increases with excitation energy, although less strongly than reported recently.[9] The observed variation of width $\Gamma$ with excitation energy $E$ (including the ground state width) can be described by the relation

$$\Gamma = A + BE^{\delta} , \tag{15}$$

with $A = 4.8$, $B = 0.0026$, and $\delta = 1.6$. Calculations[22,25] show that the observed large increase in width cannot come from increased damping at higher temperature or from a coupling to low-lying quadrupole vibrations. In a recent work[5] a calculation of the width of the GDR built on a hot rotating nucleus has been discussed. The authors find that in the spherical Sn nuclei the increase in width results mainly from the shape change to an oblate deformation at higher angular momentum and temperature due to breaking of particle correlations. A wide distribution of the magnitude of deformation due to thermal fluctuations gives rise to an average, wide strength function. The fact that the observed GDR strength function at high energies shows more structure than a single Lorentzian is qualitatively in agreement with this theory. Their calculation for $^{108}Sn$ can also be described by Eq. (15), with $A = 1.0$, $B = 0.0026$, and $\delta = 1.7$. The small value of $A$ can be attributed to the fact that the calculation does not include any damping. Although the gross comparison of this energy dependence with the experiment supports the theory, this should not be stretched too far because calculations were done for a definite energy and spin (higher at higher excitation energy).

In this context, it should also be noted that the CASCADE calculations assume the same (input) energy and width value at all decay steps and for all spin. This is certainly not justified for the width, and for an exact treatment of the problem we incorporated an energy and spin dependence of $\Gamma$ in the code CASCADE. In searching for a $(E,J)$ dependence of $\Gamma$ describing the data at all four excitation energies, it was found that it was not possible to fit the data by either only an energy dependence or only a spin dependence. This is consistent with the theory proposed in Ref. 5. Good fits

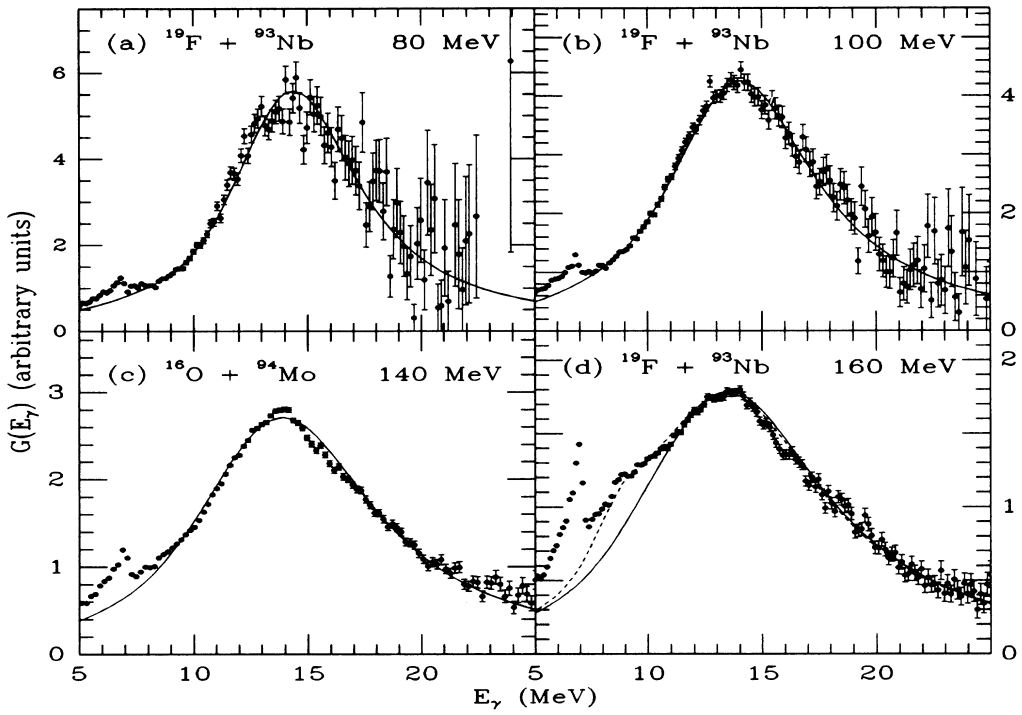


FIG. 7. The "divided plots" of the experimental data and the CASCADE fits shown in Fig. 6, at various bombarding energies. The ordinate is proportional to the strength function $G(E_\gamma)=F(E_\gamma)/E_\gamma^3$ ($F(E_\gamma)$ is defined in the text). The solid curves show the single Lorentzian fits on a linear scale. The dashed curve in (d) at 160 MeV is obtained by adding to the main Lorentzian component ($E_D=14.6$ MeV, $\Gamma_D=10.5$ MeV), another component ($E_D=8.8$ MeV, $\Gamma_D=3.0$ MeV) having 5% strength.

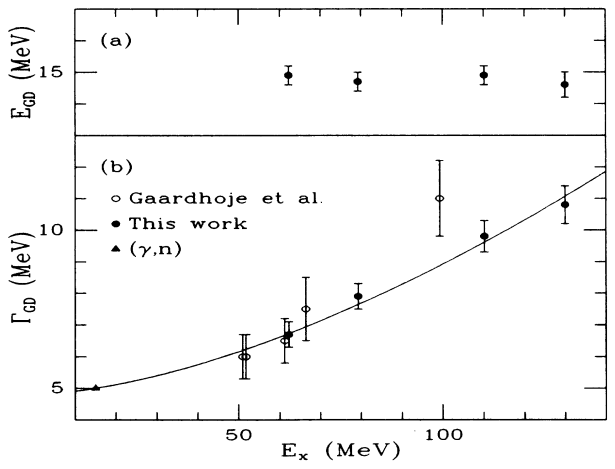


FIG. 8. Energy (a) and width (b) of the GDR extracted from the present data at different excitation energies in the compound nuclei $^{110,112}$Sn. The widths obtained in an earlier work (Ref. 9) are shown by open circles. The ground state GDR width obtained from $(\gamma,n)$ work is also indicated. The curve through the data points in (b) is described by Eq. (15) of the text.

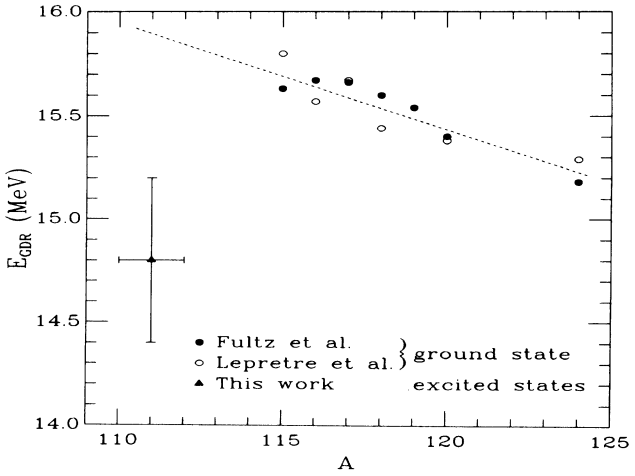


FIG. 9. Comparison of the energies of the ground state GDR's for mass $A=115-124$ and of the excited state GDR for $A=110-112$. Two available sets for ground state data (Refs. 23 and 24) are plotted. The dashed line extrapolates the ground state values to the mass region $A\sim111$. The excited state value is the average for four excitation energies obtained in this work.

were obtained for all four excitation energies by the relation,

$$\Gamma = A + BE^2 + CJ^2 \tag{15a}$$

with $A=4.5$, $B=0.0004$, and $C=0.003$. It is interesting that a linear dependence on spin also failed to reproduce the data.

At the two higher bombarding energies in the present work, the presence of incomplete fusion must be considered. A recent work[26] discusses the cross sections of complete and incomplete fusion products in the reaction $^{20}Ne + {}^{93}Nb$ at 106 and 148 MeV. If all projectile like fragments are associated with incomplete fusion (ICF) but all light particles with complete fusion (CF) one obtains a ratio $\sigma_{ICF}/\sigma_{CF} \sim 0.25$. Attributing some $\alpha$ particles to incomplete fusion raises this ratio and the highest value claimed is $\sim 0.45$. One may check these values against two systematics. Wilczynski *et al.*[27] reports a ratio of about 18% in the $^{14}N + {}^{159}Tb$ system at a comparable energy, which fits the sumrule model for fusion reactions. Secondly the velocity systematics established by Morgenstern *et al.*[28] for lighter systems may be extrapolated to the present reaction and yields a relative contribution of incomplete fusion of $\sim 20\%$ at the highest bombarding energy. In order to evaluate the effect of incomplete fusion on the extracted GDR parameters, the $\gamma$ spectrum following the incomplete fusion of 160 MeV $^{19}F$ on $^{93}Nb$ was calculated assuming that $^{16}O$ fuses with the target at a proportionally reduced energy of $\sim 132$ MeV. This is one of the most dominant incomplete fusion channels considering the sumrule model. The GDR parameters necessary for this calculation were chosen from the systematics established in this work. This spectrum was added to the one following complete fusion (calculated with the best fit parameters) with proper weight factors and the summed spectrum was compared with the experimental data. Even assuming a relative probability of 25% incomplete fusion did not change the fit.

## VI. CONCLUSIONS

The present experiments establish the existence and properties of the excited state giant dipole resonances in $A \sim 110$ nuclei in the excitation energy range 60–130 MeV (nuclear temperature $T = 1.8$–$2.7$ MeV) and angular momentum up to $\sim 60\hbar$. The extracted energy for the GDR has a value of $14.8 \pm 0.4$ MeV and is, within the errors, independent of excitation energy. It is, however, about 1 MeV below the value extrapolated from various Sn isotopes for the ground state GDR. The width of the GDR increases from a ground state value of 5 to 11 MeV at $E_x = 130$ MeV. The peak shape of the $E1$ strength function is fitted well by a single Lorentzian except at the highest excitation energy where the spectrum shows additional structure. A single component GDR is expected if the excited states of these nuclei have spherical shapes. The observed increase in the GDR width with excitation energy is qualitatively consistent with a calculation done for this mass region. According to this theory the nuclei attain oblate shapes of various deformations at high angular momentum and temperature and the GDR strength function is an average over the ensemble. The observed structure in the spectrum at the highest excitation energy supports this idea. However, the one component structure in the observed strength function suggests that on the average, the nuclei retain the spherical shape.

No convincing evidence was found for the IVGQR built on excited states. But it appears that the fusion evaporation reaction is not a sensitive probe for this high energy mode. Although the cross section for this mode increases at higher bombarding energies, the rapidly increasing width of the GDR at high excitation energy spreads the dipole strength into the region of the GQR, thus obscuring its presence.

## ACKNOWLEDGMENTS

We are thankful to P. Fröbrich for sending us the calculated fusion cross sections based on the surface friction model, for the reactions studied in this paper. This work was supported in part by the National Science Foundation.

*Permanent address: Nuclear Physics Division, Bhabha Atomic Research Center, Bombay, India.

†Present address: Department de Nucleaire–Basse energie, Centre d'Etudes Nucleaires de Saclay, F-91191 Gif-sur-Yvette, France.

‡Permanent address: The Niels Bohr Institute, University of Copenhagen, DK-2100 Copenhagen, Denmark.

[1]K. A. Snover, Annu. Rev. Nucl. Part. Sci. **36**, 645 (1986), and references cited therein.

[2]J. J. Gaardhoje, C. Ellegaard, B. Herskind, and S. G. Steadman, Phys. Rev. Lett. **53**, 148 (1984).

[3]C. A. Gossett, K. A. Snover, J. A. Behr, G. Feldman, and J. L. Osborne, Phys. Rev. Lett. **54**, 1486 (1985).

[4]D. R. Chakrabarty, M. Thoennessen, N. Alamanos, P. Paul, and S. Sen, Phys. Rev. Lett. **58**, 1092 (1987).

[5]M. Gallardo, M. Diebel, T. Dossing, and R. A. Broglia, Nucl. Phys. **A443**, 415 (1985).

[6]J. Dudek and W. Nazarewicz, Phys. Rev. C **31**, 298 (1985).

[7]A. L. Goodman, Phys. Rev. C **33**, 2212 (1986).

[8]Y. Alhassid, S. Levit, and J. Zingman, Phys. Rev. Lett. **57**, 539 (1986).

[9]J. J. Gaardhoje, C. Ellegaard, B. Herskind, R. M. Diamond, M. A. Delaplanque, G. Dines, A. O. Macchiavelli, and F. S. Stephens, Phys. Rev. Lett. **56**, 1783 (1986).

[10]S. Sen, D. R. Chakrabarty, P. Paul, J. Stachel, and M. Thoennenssen, submitted to Nucl. Instrum. Methods A.

[11]R. B. Day, Phys. Rev. **102**, 767 (1956).

[12]D. L. Hills, J. D. Garrett, O. Christensen, B. Fernandez, G. B. Hagemann, B. Herskind, B. B. Back, and F. Folkmann, Nucl. Phys. **A325**, 216 (1979).

[13]S. Y. Van der Werf, Nucl. Instrum. Methods **153**, 221 (1978).
[14]F. Puhlhofer, Nucl. Phys. **A280**, 267 (1977).
[15]R. M. Diamond and F. S. Stephens, Annu. Rev. Nucl. Part. Sci. **30**, 85 (1980).
[16]J. E. Lynn, *Theory of Neutron Resonance Reactions* (Clarendon, Oxford, 1968).
[17]R. Vandenbosch and J. R. Huizenga, *Nuclear Fission* (Academic, New York and London, 1973), p. 228.
[18]W. Swiatecki, Nucl. Phys. **A376**, 275 (1982); S. Bjornholm and W. Swiatecki, *ibid.* **A391**, 471 (1982).
[19]P. Fröbrich, Phys. Rep. **116**, 338 (1984).
[20]G. Nebbia *et al.*, Phys. Lett. **176B**, 20 (1986).
[21]F. E. Bertrand, Nucl. Phys. **A354**, 129c (1981).
[22]P. F. Bortignon, R. A. Broglia, G. F. Bertsch, and J. Pacheco, Nucl. Phys. **A460**, 149 (1986).
[23]S. C. Fultz, B. L. Berman, J. T. Caldwell, R. L. Bramblett, and M. A. Kelly, Phys. Rev. **186**, 1255 (1969).
[24]A. Lepretre, H. Beil, R. Bergere, P. Carlos, A. de Miniac, A. Veyssiere, and K. Kernbach, Nucl. Phys. **A219**, 39 (1974).
[25]A. Bohr and B. R. Mottelson, *Nuclear Structure* (Benjamin, New York, 1975), Vol. 2.
[26]D. J. Parker, J. J. Hogan, and J. Asher, Phys. Rev. C **35**, 35 (1987).
[27]J. Wilczynski, K. Siwek-Wilczynska, J. Van Driel, S. Gonggrijp, D. C. J. M. Hageman, R. V. F. Janssens, J. Lukasiak, and R. H. Siemssen, Phys. Rev. Lett. **45**, 606 (1980).
[28]H. Morgenstern, W. Bohne, W. Galster, K. Grabisch, and A. Kyanowski, Phys. Rev. Lett. **52**, 1104 (1984).